Internal structure and colloidal behaviour of covalent whey protein microgels obtained by heat treatment

Christophe Schmitt,*[a] Christian Moitzi,[b] Claudine Bovay,[a] Martine Rouvet,[a] Lionel Bovetto,[a] Laurence Donato,[a] Martin E. Leser,[a] Peter Schurtenberger[b] and Anna Stradner[b]

Covalently cross-linked whey protein microgels (WPM) were produced without the use of a chemical cross-linking agent. The hierarchical structure of WPM is formed by a complex interplay of heat denaturation, aggregation, electrostatic repulsion, and formation of disulfide bonds. Therefore, well-defined spherical particles with a diameter of several hundreds of nanometers and with relatively low polydispersity are formed in a narrow pH regime (5.8–6.2) only. WPM production was carried out on large scale by heating a protein solution in a plate-plate heat exchanger. Thereafter, the microgels were concentrated by microfiltration and spray dried into a powder. The spherical structure of the WPM was conserved in the powder. After re-dispersion, the microgel dispersions fully recovered their initial structure and size distribution. Due to the formation of disulfide bonds the particles were internally covalently cross-linked and were remarkably stable in a large pH range. Because of the pH dependent charge of the constituents the particles underwent significant size changes upon shifting the pH. Small angle X-ray scattering experiments were used to reveal their internal structure, and we report on the pH-induced structural changes occurring on different length scale. Our experiments showed that close analogies could be drawn to internally cross-linked and pH-responsive microgels based on weak polyelectrolytes. WPM also exhibited a pronounced swelling at pH values below the isoelectric point (IEP), and a collapse at the IEP. However, in contrast to classical microgels, WPM are not build up by simple polymer chains but possess a complex hierarchical structure consisting of strands formed by clusters of aggregated denatured proteins that act as primary building blocks. They were flexible enough to respond to changes of the environment, and were stable enough to tolerate pH values where the proteins were highly charged and the strands were stretched.

Introduction

Polymer-based nanogels and microgels attracted noticeable research interest during the last decade because of their wide range of potential applications as for example controlled drug delivery, immunosensing, protein purification, optics manufacturing or tissue engineering.[1,2] These colloidal particles are generally produced by emulsion or dispersion polymerisation of activated monomers in the presence of a specific solvent or reaction limiting secondary polymers (*e.g.* steric stabilizers). Microgels generally fall in the 100 to 1000 nm diameter size range as determined by microscopy or scattering techniques.[3]

An interesting class of polyampholyte microgels is obtained when a mixture of polyelectrolytes carrying carboxylic and amino groups are used as monomers.[4] This leads to stimuli responsive microgels exhibiting pH- and salt-sensitive colloidal properties such as aggregation, shrinking or swelling.[5–10]

Besides the various synthetic polyelectrolytes available for the production of polyampholyte microgels, an interesting source are food grade proteins such as bovine serum albumin (BSA) or egg albumin.[3] In this respect, it is worth mentioning that some protein microgels already exist naturally such as the well-known casein micelles.[11] The latter are cross-linked with calcium-phosphate bridges and are therefore acid sensitive. However, they can be further stabilized by covalent cross-linking using enzymatic treatment with transglutaminase.[12] Several studies also report on the use of the bovine whey proteins for production of nanogels (diameter around 60 nm) using the desolvation method for delivery purposes.[13,14]

Very recently, it was shown that stable dispersions of protein-based particles were obtained upon fast heating (> 26 °C/min) of a 1 wt% solution of demineralized β-lactoglobulin (β-lg), the major whey protein in cow milk, in a very narrow pH range of 5.8–6.2.[15] Similar structures were already described when a whey protein isolate was heated in the same conditions in the pH 6.0–6.4 range.[16] These microgels were characterized by a hydrodynamic radius ranging around 100–125 nm, a low polydispersity index (below 0.2) and a spherical shape.[15,17] They represent an intermediate aggregation state of β-lg between the already described particulates (> 1 μm) which are formed at the protein isoelectric point (IEP) at pH 5.2[18–20] and small fractal aggregates (< 100 nm) which are obtained for pH values larger than 6.6.[21–23] The self-limited aggregation of β-lg microgels within this narrow pH window can be explained by an equilibrium between attractive hydrophobic forces arising from protein denaturation and repulsive forces arising from the protein net charge.[15]

[a]*Nestlé Research Center, Department of Food Science and Technology, Vers-chez-les-Blanc, P.O. Box 44, CH-1000 Lausanne 26, Switzerland. E-mail: christophe.schmitt@rdls.nestle.com; Fax: + 41 21 785 85 54; Tel: + 41 21 785 89 36*
[b]*Adolphe Merkle Institute, University of Fribourg, Route de l'Ancienne Papeterie, P.O. Box 209, CH-1723 Marly 1, Switzerland*

Based on the results obtained with β-lactoglobulin, the aim of the present study is to explore analogies to synthetic microgels in order to better understand the complex food colloid. Covalent protein microgels were synthesised using a commercial whey protein isolate as the starting material.[24] A powdered ingredient was produced on large scale by combination of fast heat treatment in a plate-plate heat exchanger, microfiltration and spray drying. Thereafter, the powdered whey protein microgels (WPM) were re-dispersed in water and thoroughly characterized for their colloidal properties as a function of pH, *i.e.* nature of internal cross-links, solubility, ζ-potential, size, and internal structure.

Experimental

Preparation of the whey protein microgel dispersion

A 50 kg batch of WPM powder was produced. This batch was obtained by heat treatment of a dispersion of whey protein isolate, WPI (Prolacta 90, Lactalis, Retiers, France) at 4 wt% protein in softened water (160 mg.L^{-1} Na^{+}) at pH 5.9 ± 0.05 (natural pH 6.48 adjusted with 1 M HCl). The WPI dispersion was pre-heated to 60 °C and then heated to 85 °C using a Soja plate-plate heat-exchanger (PHE) operating at a flow rate of 1000 L.h^{-1}, followed by a holding time of 15 min in a tubular heat exchanger and subsequent cooling to 4 °C. Under these operating conditions, the Reynolds number Re was approx. 1,500 ensuring a laminar flow in the PHE. More than 85% of the initial proteins were converted into WPM (determined by absorbance measurements at 278 nm after removal of the WPM by centrifugation at 26,900g for 20 min). They exhibited a hydrodynamic radius of 136 ± 7 nm and a polydispersity index of 0.1 (determined by dynamic light scattering, DLS). Thereafter, the WPM dispersion was concentrated to 22 wt% by microfiltration using two Carbosep 0.14 membranes with a total surface of 6.8 m^2 (Novasep Process, Miribel, France) at a temperature of 10 °C and a flow rate of 180 L.h^{-1}. The liquid concentrate was then spray dried (feeding rate: 25 kg.h^{-1} WPM concentrate; inlet air temperature: 145–150 °C; outlet air temperature: 75–77 °C; spraying nozzle Ø: 0.5 mm; spraying pressure 40 bar) using a GEA Niro SD6.3N spray dryer (Søborg, Denmark) and stored at 10 °C in 2 kg aluminium sealed bags. The WPM powder contained 97% of the proteins in the form of microgels. Its composition was (g/100g of wet powder): protein (Nx6.38, Kjeldhal), 91; moisture, 3.6; lactose, 3; fat, 0.4 and ash, 2. Mineral composition of the powder was (g/100g of wet powder): Ca^{2+}, 0.320; K^{+}, 0.409; Na^{+}, 0.468; Mg^{2+}, 0.060; Cl^{-}, 0.178 as determined upon HNO_3/H_2O_2 mineralization of the protein sample and analysis using a Vista MPX simultaneous ICP-AES spectrometer (Varian Inc. Palo Alto, CA, USA).

For the preparation of the WPM dispersions, the WPM powder was dispersed at 4 wt% (on the protein basis) in Millipore water (resistivity = 18.2 MΩ.cm) at room temperature for 2 h under moderate stirring. Preliminary trials showed that a homogenisation treatment of the WPM dispersion at 250/50 bar was required to recover solubility and particle size distribution similar to those of the liquid WPM dispersion before spray drying. A lab scale Rannie MINI-LAB homogenizer (Kindler Maschinen AG, Zürich, Switzerland) was used to perform this processing step. After homogenization, it was checked that the morphology, hydrodynamic radius and polydispersity index of the WPM were identical to the values obtained with the liquid WPM dispersion before microfiltration and spray drying (Fig. 1 and 2). The native pH of the starting 4 wt% WPM dispersion was 6.51.

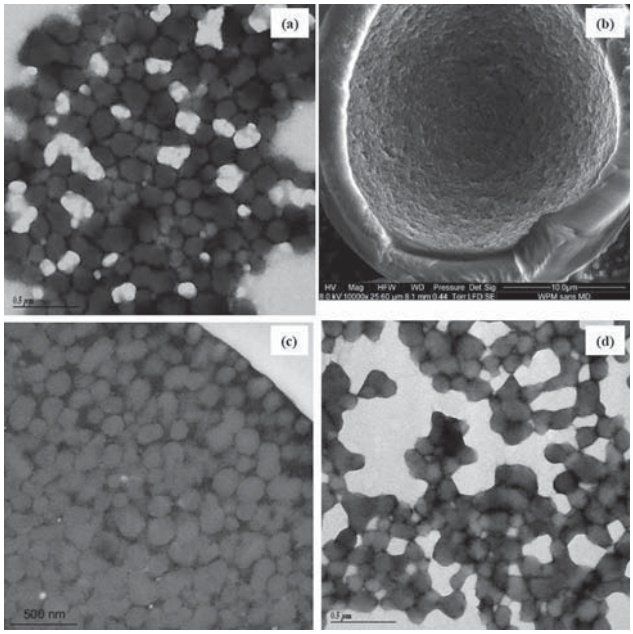

Fig. 1 (a) Negative-staining TEM micrograph from a freshly prepared 4 wt% WPM dispersion. Scale bar is 0.5 μm. (b) SEM micrograph from a WPM powder granule. Scale bar is 10 μm. (c) TEM micrograph of a thin-section from the wall of WPM powder granule. Scale bar is 500 nm. (d) Negative-staining TEM micrograph from a 4 wt% WPM dispersion reconstituted from powder after homogenization at 250/50 bar. Scale bar is 0.5 μm.

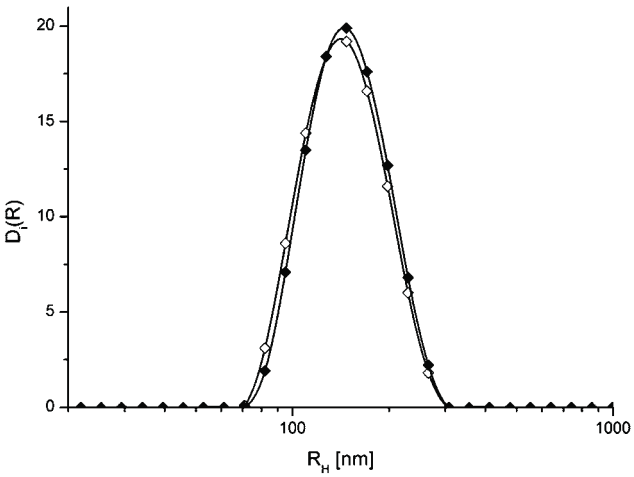

Fig. 2 Intensity weighted size distribution from a 0.4 wt% WPM dispersion measured by DLS at 25 °C. Fresh WPM dispersion: open symbols; WPM dispersion from homogenized powder: filled symbols.

For pH adjustment, 1M NaOH or HCl of analytical grade were used (Merck, Darmstadt, Germany). The denaturing agents, sodium dodecyl sulfate (SDS), urea and dithiothreitol (DTT) were of analytical grade from Fluka and Merck.

Determination of whey protein microgel morphology in dispersion and in powder

The WPM dispersion and WPM powder have been investigated by scanning electron microscopy (SEM) and transmission electron microscopy (TEM). For TEM, samples were both observed using cryofixation and embedding in Spurr resin or negative staining method.

For cryofixation and embedding in Spurr resin, 50 mg of WPM powder were dispersed in a tube containing 3 mL of a 2.5% anhydrous glutaraldehyde in methanol solution at −40 °C. The next day, 1 mL of a 20 mg/mL osmic acid in methanol was added to the tube at −40 °C and incubated for 24 h. Tubes were then transferred at 4 °C for 2 h and centrifuged for 5 min at 3500 rpm. The supernatant was removed and replaced by methanol at 4 °C. After vortexing, samples were left at 4 °C for 1 h. A similar procedure was applied replacing methanol by ethanol (2 times 1 h incubation at room temperature), mix 1 : 1 Spurr resin/ethanol at 4 °C overnight, mix 2 : 1 Spurr resin/ethanol at 4 °C 48 h, 100% Spurr resin at 4 °C. After centrifugation, the supernatant was removed and replaced by freshly prepared Spurr resin and the tube was placed under vacuum for 2 h. After storage at 4 °C and centrifugation, the bottom phase was dropped in moulds and covered with 100% Spurr resin. Polymerisation of the resin was obtained by incubation of the moulds at 70 °C for 48 h.

Semi-fine sections were stained by toluidine blue at 0.5% in Borax buffer 1% and mounted in 45% glycerol. Imaging was performed using a Zeiss Axioplan II light microscope equipped with an Axiocam camera. Ultra-thin sections were stained with uranyl acetate and lead citrate before observation under a Philips CM12 microscope operating at 80 kV. Images were recorded by a Gatan Multiscan Camera Model 794.

For the negative staining method, a drop of the WPM dispersion was deposited onto a carbon support film mounted on a copper grid. The excess product was removed after 30 s using a filter paper. A droplet of 1% phosphotungstic acid at pH 7.0 was added for 15 s, any excess being removed as before. Micrographs were made using a Philips CM12 transmission electron microscope as described before.

For SEM observation of the powders, the dry products were mounted on sample holders with double-side adhesive tape. A part of the sample was cut with a razor blade to reveal the inner structure of the particles. The samples were examined by SEM using a FEI Quanta 200F microscope at an accelerating voltage of 8 kV. The detector used was the LFD (large Field Detector) in low vacuum mode and no gold was sputtered.

Chemical stability of WPM

Internal bonds responsible for the stability of WPM have been investigated upon incubation of 1 wt% WPM dispersion in various denaturing reagents which are specifically affecting: hydrophobic interactions for SDS, hydrogen bonds for urea and disulfide bonds for dithiothreitol (DTT).[25,26] SDS and urea experiments have been performed at room temperature, whereas DTT incubation required a heat treatment at 70 °C for 15 min to be effective. In addition to the testing of single denaturing agents, WPM have been exposed to mixtures of these compounds until the resulting dispersion became transparent and the particle size determined by DLS was close to that reported for whey protein soluble aggregates obtained at pH 7.0 in similar heating conditions, *i.e.* z-average hydrodynamic radius about 20–25 nm.[16,23]

In addition, the cross-linking density of the WPM was indirectly evaluated from the loss of soluble proteins after centrifugation of the 4 wt% WPM dispersion at 26 900 g for 20 min at pH 2.0, 6.0 and 8.0. The protein contents in the supernatants were determined by UV/VIS spectroscopy (molar extinction coefficient $\varepsilon_{278} = 10.1\ g^{-1}.dL.cm^{-1}$ as determined experimentally) using a Nicolet Evolution 100 spectrometre (Sysmex Digitana SA, Switzerland).

Colloidal stability of WPM

The colloidal stability of the WPM was determined after reconstitution at 4 wt% (protein basis) by UV/VIS spectroscopy as described above. The pH of the WPM dispersion was then adjusted between 2 and 8 by addition of 1M NaOH or HCl. The absorbance of the WPM dispersion was measured at 500 nm using a Nicolet Evolution 100 spectrophotometer (Digitana, Yverdon-les-Bains, Switzerland) equipped with a 1 cm pathlength cuvette. If necessary, the sample was diluted to obtain an absorbance value below 1 absorbance unit (where variation of absorbance is linear with the number of particles for a given size). The WPM dispersion was then centrifuged at 173g for 5 min using a Sorvall RC3C Plus centrifuge (Kendro Laboratory Products, Geneva, CH) and the absorbance of the supernatant was measured. The protein solubility was expressed as the ratio between the absorbance at 500 nm before and after centrifugation normalised by the protein content of the WPM powder. All experiments were done with two independent samples.

Determination of whey protein microgel size distribution and ζ-potential

The hydrodynamic radius R_H of the WPM was measured by dynamic light scattering using a Nanosizer ZS instrument (Malvern Instruments Ltd, Worcestershire, UK). The instrument was used in the backscattering configuration. Samples were diluted to a protein concentration of 0.4 wt% and placed in a square quartz cell (Hellma 282 QS, Germany, pathlength 1 cm). The hydrodynamic radius and the polydispersity index were calculated by a cumulant analysis of the autocorrelation function.[27]

The ζ-potential of the WPM was determined between pH 2.0 and 8.0 by light scattering upon application of an alternating electrical field into a disposable capillary cell (DTS 1060, Malvern Instruments Ltd, Worcestershire, UK) at a protein concentration of 0.1 wt%. The Nanosizer ZS apparatus was used in its ζ-potential measurement mode at 25 °C. The effective electrical field, E, applied in the measurement cell varied between 50 and 150 V depending on the ionic strength of the samples. The overall electrophoretic mobility, μ, was calculated assuming spherical particles.[28] The ζ-potential was then calculated using the Smoluchoski equation. The accuracy of the measurement of the ζ-potential was probed with a standard solution (DTS1050, Malvern Instruments Ltd, Worcestershire, UK) giving a value of -50 ± 5 mV.

Determination of the internal structure of whey protein microgels

The small angle X-ray scattering (SAXS) experiments were done at the Swiss Light Source (Paul Scherrer Institute, Switzerland) at the cSAXS instrument. Samples of 4 wt% WPM at pH ranging from 2.0 to 8.0 were measured in 1 mm quartz capillaries at 20 °C. The protein concentration was corrected for dilution induced by pH adjustment below and above pH 6.51 (natural pH of WPM dispersion). At least fifty 2D images were taken, azimuthally integrated and averaged according to established procedures provided by the Paul Scherrer Institute. The q-scale was calibrated by a measurement of silver behenate. Absolute calibration was done by measuring the scattered intensity of water, which depends only on the isothermal compressibility and on the electron density ($I(0)_{water,25°C} = 0.01633\ cm^{-1}$).[29]

Results and discussion

Structure and physicochemical interactions in whey protein microgels

The morphology of whey protein microgels (WPM) was investigated before and after spray drying using transmission and scanning electron microscopy (Fig. 1). Fig. 1a and 1d show that WPM exhibit a spherical shape and a quite high density as estimated from the strong contrast between the particles and the background upon staining. The particles had the tendency to aggregate on the observation grid, but they remained stable in solution. Interestingly, the morphology of the WPM was not markedly affected by the spray drying treatment and homogenisation at 250/50 bar. Based on TEM pictures, the diameter of the WPM ranged between 120 to 300 nm which was slightly lower compared to the light scattering data, but might be due to a slight dehydration of the WPM during the sample treatment for TEM experiments. These values are slightly larger than those reported for pure β-lg microgels obtained at 1 wt% under similar heating conditions,[15,17] but the difference could be due to the fourfold higher protein concentration used here as well as due to the use of an industrial plate heat exchanger rather than a water bath for performing the heat treatment step as well as to the mineral composition of the whey protein isolate.[24] The appearance and size of the WPM were similar to those of the casein micelles held together by calcium phosphate bridges or internally cross-linked with the transglutaminase enzyme,[12,35] but also to that of synthetic microgels such as copolymers of poly-(methacrylic acid) and poly(2-(diethylamino)ethyl methacrylate) (PMAA/PDEA)[36] or lightly cross-linked sterically stabilized poly(2-vinylpiridine) latexes.[37]

The analysis of the WPM powder by SEM revealed that microgels were packed into spherical hollow particles having a diameter of 30–40 μm formed by water evaporation during the spray-drying step. This led to a granular internal surface of the powder granules (Fig. 1b). At a larger magnification using resin embedding/sectioning and TEM, the internal structure of the powder particle could be better resolved (Fig. 1c). WPM were densely packed within the wall of the powder granule, but they were keeping their globular shape without exhibiting noticeable fusion. The volume fraction occupied by the whey protein microgels within the powder granule was about 60–70%, which corresponds to the expected packing given by random close packing of hard spheres.

The stability of the whey protein microgels to spray drying and subsequent homogenization treatment was also investigated by dynamic light scattering on dilute dispersions (Fig. 2). It could be seen that the size distribution obtained for the fresh WPM dispersion before spray drying matched with the one of the WPM dispersion prepared by homogenization of the spray dried powder. Calculation of the z-average hydrodynamic radii resulted in 136 ± 7 nm for the "fresh" WPM (polydispersity index: 0.1) and 142 ± 3 nm for the powdered and re-dispersed ones (polydispersity index: 0.07), which agreed with the radii estimated from the TEM micrographs.

In a next step, the bonds responsible for the stability of the WPM were probed in presence of a series of denaturing agents: sodium dodecyl sulfate (SDS), urea and dithiothreitol (DTT). Combined urea and SDS were not able to dissociate WPM, revealing that not only hydrogen and hydrophobic bonds were present. However, when urea or SDS were combined with DTT, an agent which is reducing disulfide bonds, WPM could be dissociated, resulting in transparent stable solutions. For example, the treatment of 1 wt% WPM with 50 mM DTT and 4 M urea led to the formation of so-called soluble aggregates[16] exhibiting a z-average hydrodynamic radius of about 40 nm (Fig. 3). These soluble aggregates most likely correspond to the building blocks of the WPM under the denaturating conditions that were used in this study.[17]

Based on the above experiments we propose the following mechanism for the formation of WPM. Upon heat denaturation the unfolded whey proteins expose hydrophobic regions which associate depending on the external physicochemical conditions, pH and protein concentration used. The quick formation of small aggregates is followed by aggregation which leads to the formation of particles that are primarily maintained by hydrophobic and hydrogen bonds (as already described for whey protein gels formed under neutral pH conditions).[25,38] Subsequently, intra-particle disulfide bonds are formed, leading to a covalent stabilisation of the structure.[39–41] The sum of all these

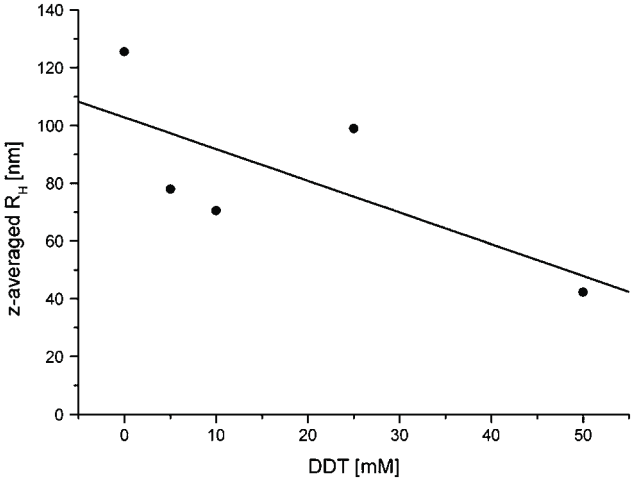

Fig. 3 Variation of the z-average hydrodynamic radius from a 1 wt% WPM dispersion after incubation with an increasing content of DDT in the presence of 4 M urea at 70 °C for 15 min.

interactions explains the remarkable stability of the whey protein microgels against physical treatments such as spray drying and homogenization. Further measurements by UV/VIS spectrophotometry revealed that only about 6.2% of the total protein content were released from the microgels at pH 2.0, 6.0 or 8.0, confirming that the cross-linking density within the WPM was high.[42]

Colloidal stability and internal structure of whey protein microgels as a function of pH

The stability of 4 wt% WPM dispersion was investigated between pH 2.0 and 8.0. Whey protein microgels were forming stable dispersions for most of the pH values tested with the exception of the range 4.0 < pH < 5.5, where they were found to be unstable, leading to precipitation (dashed area on Fig. 4). In order to shed more light on the pH-dependent stability, the variation of the ζ-potential of the microgels was measured as a function of pH. Fig. 4 shows that the WPM exhibited a polyampholyte character around a critical pH value of 4.82 (isoelectric point; IEP) for which the overall surface charge was zero. Below this pH value, WPM were positively charged, above they were negatively charged. The samples were stable against aggregation/precipitation when the ζ-potential exceeded an absolute value of 20 mV.[43] This limit was reached at pH values below 4.0 and above 5.5. From these results, it could be concluded that the colloidal stability of the whey protein microgels was mainly controlled by their overall charge. This charge resulted from the balance between the dissociation of carboxylic and amino groups of the whey protein side chains as a function of pH. In the pH region between 4.0 and 5.5, electrostatic repulsion between individual microgels was too low to provide colloidal stability. Thus, WPM aggregation and precipitation occurred. Such pH-sensitive behaviour is typical for polyampholyte microgels and was recently described for synthetic polyampholyte microgels of 40% poly(methacrylic acid) and 60% poly(2-(diethylamino)ethyl methacrylate) (PMAA/PDEA) having an isoelectrical pH of about 5.0.[36] A similar pH-behaviour was also reported for 150–280 nm human serum albumin microgels with an IEP of 5.0 that were produced by desolvation in ethanol and cross-linking using glutaraldehyde.[13]

The internal structure of whey protein microgels was investigated by means of SAXS. Despite the relatively large protein concentration, we did not see significant interaction effects. This could be explained by the relatively large polydispersity of WPM and by the limited q-range accessible by SAXS. The experimental scattering curves at three selected pH values are shown in Fig. 5a. Overall the data exhibited no dramatic changes upon variation of the pH, highlighting the internal stability of the microgels between pH 2.0 and 8.0. Nevertheless, changes in the position of a clearly visible shoulder at approx. 0.05 nm^{-1} and in the slope of the scattering curve for $q \geq 0.1$ nm^{-1} were observed. A closer look at the high-q behaviour furthermore revealed the presence

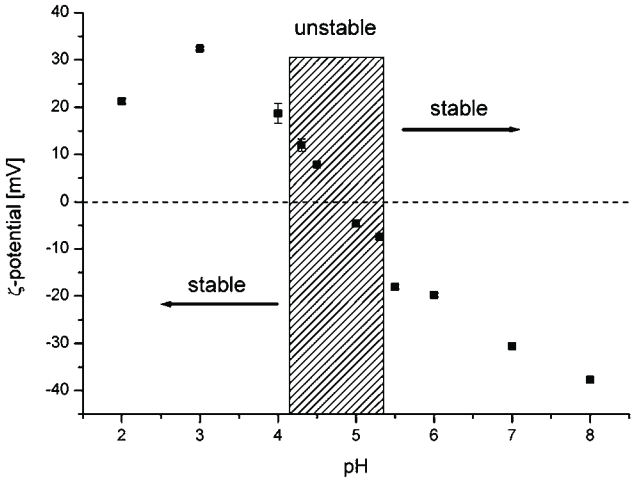

Fig. 4 Variation of the ζ-potential from a 0.1 wt% WPM dispersion at 25 °C as a function of pH. The vertical line indicates ζ-potential value of zero. Vertical bars indicate standard deviation. The dashed area is indicating the pH regime where WPM aggregate. In the stable regions the WPM solubility is larger than 90% while in the aggregated regime it is below 5%.

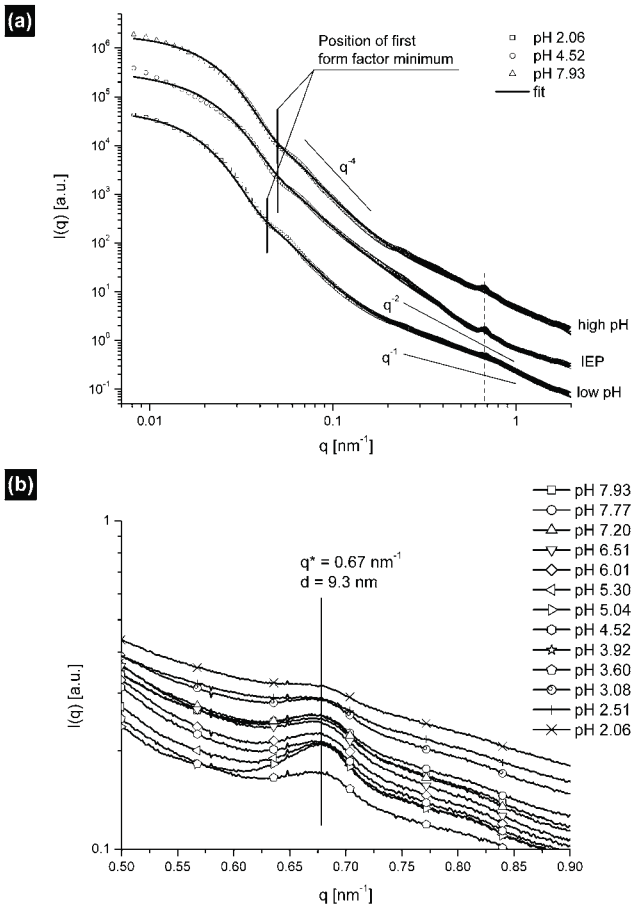

Fig. 5 (a) SAXS curves obtained from 4 wt% WPM dispersions at selected pH values after subtraction of the solvent scattering. The curves are shifted vertically for better visibility. The fitting model consisted of a lognormal distribution of homogeneous spheres plus a power law decay of the intensity due to the internal fractal structure. The samples close to the IEP show an upturn of the scattered intensity at very small q-values due to aggregation. The fitted curve deviates from the experimental data in this regime. (b) Enlargement of the high q region of the SAXS curves showing the presence of a correlation peak at $q = 0.67$ nm^{-1}.

of a correlation peak located at a scattering vector q $\approx$ 0.67 nm^{-1} (Fig. 5b).

The general features of the scattering curve expected for particles with various structures are depicted in Scheme 1. They were used to interpret qualitatively the data shown in Fig. 5. At small scattering vectors, the data are primarily expected to reflect the overall size and shape of the WPM. At larger q-values, where the scattering experiment now probes a reduced characteristic length scale (given by $2\pi/q$), the contributions from the inner structure of the WPM on these length scales are primarily observed. As the internal structure is proposed to be fractal, a power-law decay of the scattering curve should be observed. The slope or fractal dimension is directly related to the compactness of the aggregate, where densely packed structures give rise to a scattering intensity which is decaying more steeply than more open structures with a smaller fractal dimension. The limiting case of a fractal dimension of 1 corresponds to a situation where the strands are stretched and are locally becoming cylindrical.[30,31]

The qualitative features of Scheme 1 could be incorporated in a scattering function suitable for a quantitative analysis of the experimental data. Here two major structural contributions from the overall spherical shape and from the internal fractal structure were assumed, respectively. The overall shape and size distribution of the microgels could be modelled by a log-normal distribution of spheres leading to the typical form factor with minima and maxima and a Porod-law at high q arising from the outer surface and is given by a power law decay of the form $I(q) \sim q^{-4}$. On a smaller length scale, the interior of the particles is not homogeneous anymore but is modelled as a fractal aggregate, which can be approximated by a power law of the form $I(q) \sim q^{-\alpha}$.

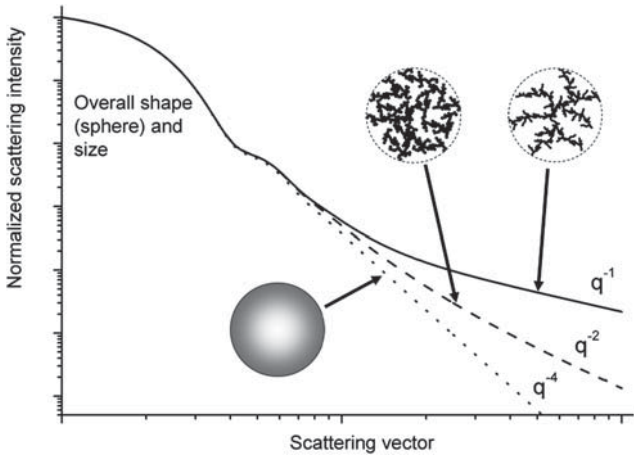

Scheme 1 Theoretical scattering curve that results from a combination of a form factor of polydisperse spheres (10% polydispersity) and a contribution from the fractal internal structure of the microgel. At small scattering vectors the curve is dominated by the overall size and shape of the particles. At larger q-values the contribution of the fractal internal structure becomes important, leading to a power-law decay of the scattering curve. Relatively densely packed aggregates (*e.g.* fractal dimension of 2) give raise to a scattering curve which is decaying steeper (q^{-2}) than more open structures with smaller fractal dimensions. The limiting case of a fractal dimension of 1 corresponds to a situation where the strands are stretched and are locally becoming cylindrical.

That leads to the following mathematical expression than can subsequently be used for fitting the experimental scattering curves:

$$I(q) = I(q)_{\text{sphere}} + c_1 q^{-\alpha} + c_2 \quad (1)$$

where $I(q)_{\text{sphere}}$ is the scattering intensity from polydisperse spheres, and c_1, c_2 and the fractal dimension α are fitting parameters needed to reproduce the contributions from the internal WPM structure.

From our SAXS data, it was clear that the WPM changed their overall size with pH. Qualitatively this could be directly seen in the scattering curves when looking at the shift of the form factor minimum at approx. 0.05 nm^{-1} (see Fig. 5a). This minimum moved to lower q-values when the pH shifted away from the IEP, reflecting an increase in particle size. The quantitative results of the model fitting for the size distributions are reported in Fig. 6. The minimum size was found to be close to the IEP. Using the analogy to polyelectrolyte microgels, swelling was expected away from the IEP as a result of the internal electrostatic repulsion between the charges present above or below the IEP. It became apparent that the WPM size increased dramatically when going to low pH values, whereas the size increase at high pH seemed much less pronounced. However, a further increase of the pH above 8 also leads to a significant increase of the size (data not shown), but ultimately to WPM disruption due to alkaline hydrolysis.

From the above it becomes immediately clear that the analysis of the scattering data shown in Fig. 6 was also done in the pH range close to the IEP where the particles were unstable and aggregated. This is reflected in the fact that for these samples the scattering intensity at very small q-values deviates from the fit due to the presence of aggregates (Fig. 5a). However, as the overall structure of the individual WPM in the aggregates did not change, the size and polydispersity of the individual particles could be determined with our fitting routine. Results showed that while the size of the WPM reflected the de-swelling and swelling cycle when increasing the pH, the polydispersity of the particle radius did not change significantly with pH.

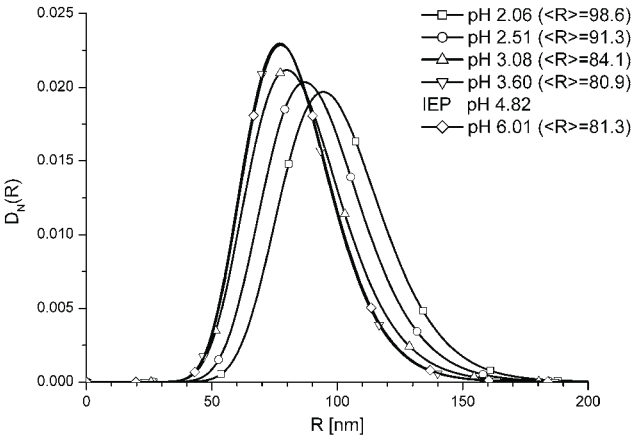

Fig. 6 Size distribution functions obtained by fitting a log-normal distribution of homogeneous spheres to the SAXS curves. The pronounced increase in size when going from the IEP towards lower pH values can clearly be seen.

The internal structure of the WPM was mainly reflected in the decay of the scattering curve at large q-vectors above 0.1 nm^{-1}. Our fitting procedure revealed a significant change in the slope of the decay α, corresponding to the fractal dimension of the particle interior (Fig. 7).

The pH at which the particles where synthesized (pH 5.9) was close to the IEP. Thus the particles were carrying only a small number of charges. The fractal dimension of the WPM interior was approximately 2.1 at this pH. This agrees well with typical values for reaction limited cluster aggregation (RLCA).[44,45] After the heat treatment during synthesis, which includes covalent cross-linking of the proteins, the pH could be changed in a wide range without dismantling the particles. When the pH was shifted towards the IEP at approx. pH 5, the particles lost their colloidal stability and reversibly aggregated. When the pH was shifted away from the IEP, the particles remained stable. The internal structure also responded to changes of the overall charge. In analogy to microgels build up by weak polyelectrolytes, the WPM were swelling when the net charge increased. Due to enhanced electrostatic repulsion of the strands of the aggregates, these strands locally stiffened and stretched, and the WPM subsequently swelled and their overall size increased. In the scattering curve these changes in the internal structure were reflected in the decrease of the slope at high q-values. At pH values below 3 a decay of the scattering curve with approx. q^{-1} was measured. This slope is characteristic for rigid rods. Thus, under conditions far away from the IEP, where the proteins are highly charged, the strands of the fractal aggregate appear strongly stretched on the length scales probed by the experiment.

It is interesting to also look more closely at the correlation peak that is clearly visible at q $\approx$ 0.67 nm^{-1}. This correlation peak corresponded to a real-space distance of about 9.2 nm, which could be related to the internal organization of the denatured whey protein monomers within the microgel (see Scheme 1). Interestingly, the correlation peak was present for all the tested pH values, but it was particularly pronounced at pH 5.0, *i.e.* around the isolelectric pH of the microgels (Fig. 5b). Under these conditions of charge neutrality, attractive interactions between the building blocks are dominating as already reported for lysozyme/polystyrene sulfonate microgels.[46] This led to a situation where the average number of nearest neighbours is higher compared to the case where the building blocks are highly charged. Thus, the structure peak was most pronounced close to the IEP.

These structural findings were confirmed by a model-independent alternative way to analyze the SAXS curves using Indirect Fourier Transformation (IFT).[32,33] This procedure results in a so-called Pair Distance Distribution Function (PDDF), which is characteristic for the size and the shape of the scattering particles[34] (Fig. 8). Using this method, aggregated samples were immediately identified as they did not exhibit the typical asymmetric bell-like shape of polydisperse particles, but exhibited a shoulder at large distances. The maximum of the PDDF (R_{max}) is directly related to the mean radius of the objects.[34,47] As in model fitting, the swelling-deswelling behaviour of the microgels was clearly visible. The swelling was estimated from the variation of R_{max} as a function of pH. A minimum of R_{max} was found at the IEP of the microgels (pH = 4.82), whereas an increase arose for high and low pH values. The IFT results also reveal the asymmetric swelling behaviour of the WPM that was already found when fitting our data with the function given in eqn (1). The swelling is marked for the acidic pH values where R_{max} increases by more than 15% (pH 2.0), leading to a 40% increase in the WPM volume. Such behaviour is very characteristic for cross-linked amphiphilic polymer microgels,[8,36] but it was also described for gels of proteins such as egg albumin[48] or whey protein concentrate.[14] The likely explanation for this behaviour is that the chains repel each other within the microgels at pH values far from the IEP where the protein is highly charged due to full protonation of the NH_3^+ groups at low pH or the deprotonation of the COO^- groups at high pH values. As the distribution of these functional groups is not symmetrical on

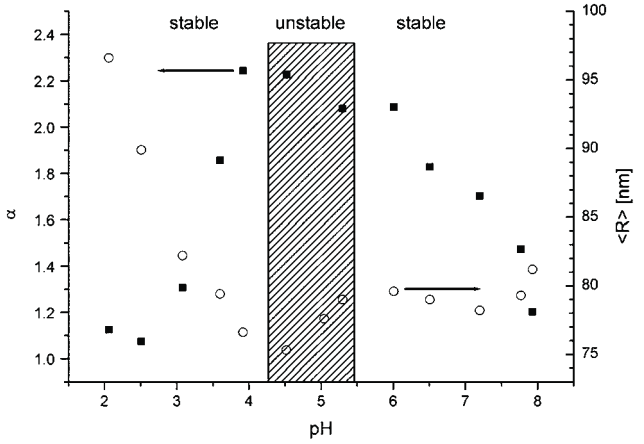

Fig. 7 Fractal dimension α of the internal structure of WPM determined from the slope of the SAXS at high angles (full symbols). The transition from relatively compact aggregates ($\alpha > 2$) close to the IEB towards swollen and expanded particles ($\alpha \sim 1$) far away from the IEP can be seen. The open symbols indicate the mean particle radius as a function of the pH.

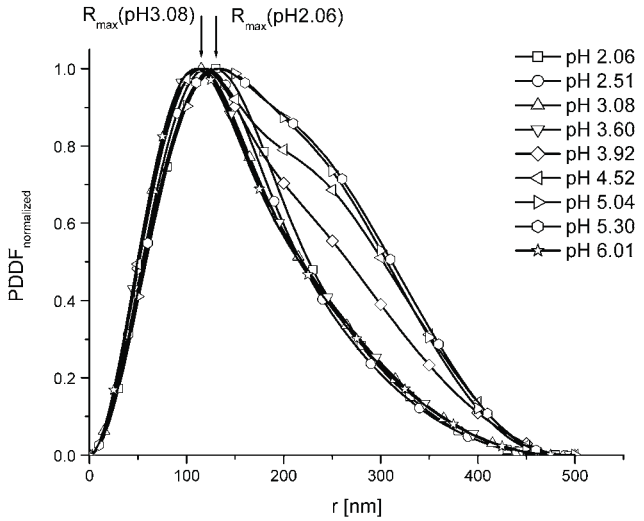

Fig. 8 Normalized pair-distance distribution functions obtained by an inverse Fourier transformation of the SAXS curves at various pH. R_{max} is indicated for two specific pH values.

both sides of the IEP of the β-lactoglobulin monomer,[49] it explains the more pronounced swelling of the microgels on the acidic side of the IEP.

Conclusions

This work is presenting a detailed structural characterization of whey protein microgels produced on a large scale with commercially available whey protein isolate. Due to the covalent internal cross-linking of the proteins, the resulting particles are remarkably stable in a very large pH regime. Only at pH values above 10, where disulfide bridges are broken, they disintegrate. Our scattering experiments have clearly revealed that these WPM are hierarchically structured (Scheme 2), which can at least qualitatively be understood on the basis of the synthesis procedure used. Upon heat denaturation the unfolded whey proteins expose hydrophobic residues towards the water and correspondingly start to aggregate. The initial quick formation of small primary aggregates is followed by fractal aggregation, which leads to the formation of larger particles that are primarily held together by hydrophobic and hydrogen bonds. Subsequently, intra-particle disulfide bonds are formed, leading to a covalent stabilisation of the structure. By microfiltration and spray drying a powder can be produced which can be perfectly redispersed in water after homogenization.

Due to the combination of electrostatic and steric repulsions these particles have a high colloidal stability except in a pH regime close to the IEP where the ζ-potential is smaller than 20 mV, where the WPM exhibit reversible aggregation. The internal structure is flexible enough to respond to changes in the solvent pH. This can be observed by a significant variation of the particle size upon shifting the pH and by a simultaneous change of the internal fractal dimension (Scheme 2). At the pH where the synthesis is done, the fractal dimension of the internal structure agrees nicely with typical values found for reaction limited cluster aggregation. At very low pH values, however, the strands of the aggregate appear to be stretched. This can be explained by the large internal charge density which is causing the aggregate to expand as much as possible.

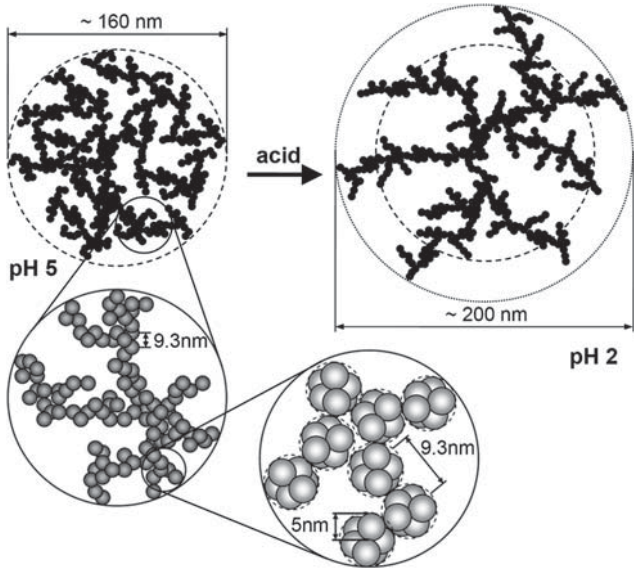

Scheme 2 WPM particles posses a hierarchically structured interior. Upon heating of the whey protein solution close to the IEP, the proteins denature (characteristic size ~ 5 nm) and rapidly form intermediate dense aggregates (characteristic size ~ 9 nm) which further aggregate to WPM. Due to the formation of intermolecular disulfide bonds the aggregates are covalently cross-linked and are stable in a large pH range. Upon shifting the pH away from the IEP, the particles swell due to intra-particle electrostatic interactions between charges on the primary aggregates that cause the network to stiffen and expand.

It is certainly interesting to consider the similarity in the aggregation and swelling-deswelling behaviour with those of microgels build up by weak polyelectrolytes. This close analogy not only helps us in understanding the structural properties of the WPM, but suggests that similar to synthetic microgels they could also be suitable for controlled release applications of active molecules. These naturally cross-linked edible protein-based microgels might thus represent a powerful tool for delivery purposes in food applications.[50] We have thus also started an investigation of the functional properties of WPM, that also includes their flow behaviour in the presence of other food macromolecules.

Acknowledgements

Marie-Lise Dillmann (Nestlé Research Center, NRC) is thanked for her technical assistance during the TEM experiments. Rafael Berrocal, Klaus Indermühle (Nesté Product Technology Centre Konolfingen) and Alain Fracheboud (NRC) are thanked for their technical assistance during the large scale preparation of the WPM powder. We thank the Adolphe Merkle Foundation, the University of Fribourg and Nestlé for financial support. The SAXS experiments were performed on the cSAXS beamline at the Swiss light source, Paul Scherrer Institute, Villigen, Switzerland. We are grateful to our local contact Andreas Menzel.

References

1 N. B. Graham and A. Cameron, *Pure Appl. Chem.*, 1998, **70**, 1271–1275.
2 D. M. Heyes and A. C. Branka, *Soft Matter*, 2009, **5**, 2681–2685.
3 H. Kawaguchi, *Prog. Polym. Sci.*, 2000, **25**, 1171–1210.
4 S. Wen and W. T. K. Stevenson, *Colloid Polym. Sci.*, 1993, **271**, 38–49.
5 M. Stieger, W. Richtering, J. S. Pedersen and P. Lindner, *J. Chem. Phys.*, 2004, **120**, 6197–6206.
6 K. Kratz, T. Hellweg and W. Eimer, *Polymer*, 2001, **42**, 6631–6639.
7 I. Berndt, J. S. Pedersen and W. Richtering, *Angew. Chem., Int. Ed.*, 2006, **45**, 1737–1741.
8 K. Ogawa, A. Nakayama and E. Kokufuta, *Langmuir*, 2003, **19**, 3178–3184.
9 J. I. Amalvy, E. J. Wanless, Y. Li, V. Michailidou and S. P. Armes, *Langmuir*, 2004, **20**, 8992–8999.
10 B. H. Tan and K. C. Tam, *Adv. Colloid Interface Sci.*, 2008, **136**, 25–44.
11 C. G. de Kruif and C. Holt, in *Advanced dairy chemistry, Vol. 1: Proteins* (3rd ed.) (Fox, P. F. and McSweeney, P. L. H., ed.), Kluwer Academic/Plenum Publishers, New York, 2003, pp 233–276.
12 T. Huppertz and C. G. de Kruif, *Int. Dairy J.*, 2008, **18**, 556–565.
13 K. Langer, S. Balthasar, V. Vogel, N. Dinauer, H. von Briesen and D. Schubert, *Int. J. Pharm.*, 2003, **257**, 169–180.
14 S. Gunasekaran, S. Ko and L. Xiao, *J. Food Eng.*, 2007, **83**, 31–40.
15 C. Schmitt, C. Bovay, A.-M. Vuilliomenet, M. Rouvet, L. Bovetto, R. Barbar and C. Sanchez, *Langmuir*, 2009, **25**, 7899–7909.
16 C. Schmitt, C. Bovay, M. Rouvet, S. Shojaei-Rami and E. Kolodziejczyk, *Langmuir*, 2007, **23**, 4155–4166.

17 L. Donato, C. Schmitt, M. Rouvet and L. Bovetto, *Int. Dairy J.*, 2009, **19**, 295–306.
18 M. Stading, M. Langton and A.-M. Hermansson, *Food Hydrocolloids*, 1993, **7**, 195–212.
19 E. H. C. Bromley, M. R. H. Krebs and A. M. Donald, *Eur. Phys. J. E*, 2006, **21**, 145–152.
20 A. M. Donald, *Soft Matter*, 2008, **4**, 1147–1150.
21 P. Aymard, D. Durand and T. Nicolai, *Int. J. Polym. Anal. Charact.*, 1996, **2**, 115–119.
22 C. Le Bon, T. Nicolai and D. Durand, *Int. J. Food Sci. Technol.*, 1999, **34**, 451–465.
23 S. Mehalebi, T. Nicolai and D. Durand, *Int. J. Biol. Macromol.*, 2008, **43**, 129–135.
24 C. Schmitt, C. Bovay, A.-M. Vuilliomenet, M. Rouvert and L. Bovetto, *Food Hydrocolloids*, 2010, DOI: 10.1016/j.foodhyd.2010.05.010.
25 J. Gezimati, L. K. Creamer and H. Singh, *J. Agric. Food Chem.*, 1997, **45**, 1130–1136.
26 P. Havea, A. J. Carr and L. K. Creamer, *J. Dairy Res.*, 2004, **71**, 330–339.
27 D. E. Koppel, *J. Chem. Phys.*, 1972, **57**, 4814–4820.
28 R. W. O'Brien, *J. Fluid Mech.*, 1988, **190**, 71–86.
29 D. Orthaber, A. Bergmann and O. Glatter, *J. Appl. Crystallogr.*, 2000, **33**, 218–225.
30 W. Burchard, *Advances in Polymer Science, Vol. 143*, Springer, Berlin/Heidelberg, 1999, pp 114–194.
31 P. Lindner and T. Zemb, *Neutrons, X-rays and Light: Scattering Methods Applied to Soft Condensed Matter*, Elsevier, Amsterdam, 2002.
32 O. Glatter, *J. Appl. Crystallogr.*, 1977, **10**, 415–421.
33 O. Glatter, in *Small Angle X-ray Scattering* (Glatter, O. and Kratky, O., ed.), Academic Press, London, 1982, pp 119–165.
34 O. Glatter, *J. Appl. Crystallogr.*, 1979, **12**, 166–175.
35 D. J. McMahon and W. R. McManus, *J. Dairy Sci.*, 1998, **81**, 2985–2993.
36 B. H. Tan, P. Ravi, L. N. Tan and K. C. Tam, *J. Colloid Interface Sci.*, 2007, **309**, 453–463.
37 S. Fujii, D. Dupin, T. Araki, S. P. Armes and H. Ade, *Langmuir*, 2009, **25**, 2588–2592.
38 K. Shimada and J. C. Cheftel, *J. Agric. Food Chem.*, 1989, **37**, 161–168.
39 D. Galani and R. K. Owusu Apenten, *Int. J. Food Sci. Technol.*, 1999, **34**, 467–476.
40 A. C. Alting, R. J. Hamer, C. G. de Kruif and R. W. Visschers, *J. Agric. Food Chem.*, 2000, **48**, 5001–5007.
41 A. C. Alting, H. H. J. de Jongh, R. W. Visschers and J.-W. F. A. Simons, *J. Agric. Food Chem.*, 2002, **50**, 4682–4689.
42 B. H. Tan, K. C. Tam, Y. C. Lam and C. B. Tan, *Adv. Colloid Interface Sci.*, 2005, **113**, 111–120.
43 A. Fernandez-Nieves and F. J. De Las Nieves, *Colloids Surf., A*, 1999, **148**, 231–243.
44 W. C. K. Poon and M. D. Haw, *Adv. Colloid Interface Sci.*, 1997, **73**, 71–126.
45 D. Asnaghi, M. Carpineti, M. Giglio and M. Sozzi, *Phys. Rev. A: At., Mol., Opt. Phys.*, 1992, **45**, 1018–1023.
46 G. Gummel, F. Boué, D. Clemens and F. Cousin, *Soft Matter*, 2008, **4**, 1653–1664.
47 C. Moitzi, I. Portnaya, O. Glatter, O. Ramon and D. Danino, *Langmuir*, 2008, **24**, 3020–3029.
48 H.-Y. Park, I.-H. Song, J.-H. Kim and W.-S. Kim, *Int. J. Pharm.*, 1998, **175**, 231–236.
49 F. Fogolari, L. Ragona, S. Licciardi, S. Romagnoli, R. Michelutti, R. Ugolini and H. Molinari, *Proteins: Struct., Funct., Genet.*, 2000, **39**, 317–330.
50 L. Chen, G. E. Remondetto and M. Subirade, *Trends Food Sci. Technol.*, 2006, **17**, 272–283.